Cell

Excitatory Local Circuits and Their Implications for Olfactory Processing in the Fly Antennal Lobe

Yuhua Shang,[1] Adam Claridge-Chang,[1] Lucas Sjulson,[1] Marc Pypaert,[1] and Gero Miesenböck[1,*]
[1] Department of Cell Biology, Yale University School of Medicine, 333 Cedar Street, New Haven, CT 06520, USA
*Correspondence: gero.miesenboeck@yale.edu
DOI 10.1016/j.cell.2006.12.034

SUMMARY

Conflicting views exist of how circuits of the antennal lobe, the insect equivalent of the olfactory bulb, translate input from olfactory receptor neurons (ORNs) into projection-neuron (PN) output. Synaptic connections between ORNs and PNs are one-to-one, yet PNs are more broadly tuned to odors than ORNs. The basis for this difference in receptive range remains unknown. Analyzing a *Drosophila* mutant lacking ORN input to one glomerulus, we show that some of the apparent complexity in the antennal lobe's output arises from lateral, interglomerular excitation of PNs. We describe a previously unidentified population of cholinergic local neurons (LNs) with multiglomerular processes. These excitatory LNs respond broadly to odors but exhibit little glomerular specificity in their synaptic output, suggesting that PNs are driven by a combination of glomerulus-specific ORN afferents and diffuse LN excitation. Lateral excitation may boost PN signals and enhance their transmission to third-order neurons in a mechanism akin to stochastic resonance.

INTRODUCTION

Although the vertebrate and insect lineages diverged in the distant evolutionary past, species of the two phyla possess olfactory systems with remarkably similar architectures. In both vertebrates and insects, the receptive range of each sensory neuron is determined by the expression of one functional member of a large family of odorant receptors (Buck and Axel, 1991; Clyne et al., 1999; Vosshall et al., 1999). The neuron's receptor choice is linked to the selection of a glomerular target in the olfactory bulb (of vertebrates) or the antennal lobe (of insects) to which its axon projects: the axons of all olfactory receptor neurons (ORNs) expressing the same odorant receptor converge onto the same glomerulus (Ressler et al., 1994; Vassar et al., 1994; Mombaerts et al., 1996; Gao et al., 2000; Vosshall et al., 2000). Signals from different odorant receptors are thus spatially segregated at the first synaptic relay in the brain.

The topographic maps established by the spatially segregated ORN projections are read by second-order principal neurons, which are termed projection neurons (PNs) in insects and mitral cells in vertebrates. In flies and rodents, the majority of second-order neurons extend dendrites into only a single glomerulus and thereby couple monosynaptically to a single class of ORNs (Stocker et al., 1990; Buonviso et al., 1991; Jefferis et al., 2001). The one-to-one connectivity of specific classes of ORNs with specific classes of PNs has suggested the existence of many independent transmission lines, each dedicated to signals from just one type of odorant receptor. Such an arrangement of many parallel but differently tuned communication channels—so-called labeled lines—permits a direct encoding of stimulus properties into neuronal identities: an odor is represented, in the simplest case, in the totality of transmission lines it activates.

Receptor signals conveyed by labeled lines are fed into processing hierarchies of increasing convergence, which enable higher-order cells to combine information carried separately in lower-order units. It is a matter of intense debate whether the antennal lobes themselves are integral parts or mere front ends of such a processing hierarchy. Optical imaging experiments in flies expressing the genetically encoded activity sensors synapto-pHluorin (spH) or G-CaMP seemed to support the latter possibility: stimulating the ORN afferents to a given set of glomeruli was found to elicit activity in PNs extending dendrites into the same set of glomeruli (Ng et al., 2002; Wang et al., 2003). This was interpreted to suggest that PNs, the antennal lobe's output neurons, retain the labeled-line format of the lobe's ORN input. However, proof that individual PNs are excited only by their cognate ORNs is lacking, as differences in ORN and PN tuning could have remained undetected in these experiments. The spH study used odor blends that activated large fractions of ORN afferents, potentially masking any input pooling by PNs (Ng et al., 2002). In the G-CaMP study, the sensor's high response threshold required odor stimuli of up to 40% saturated vapor to elicit detectable signals in a handful of glomeruli (Wang et al., 2003). Indeed, electrophysiological recordings from single

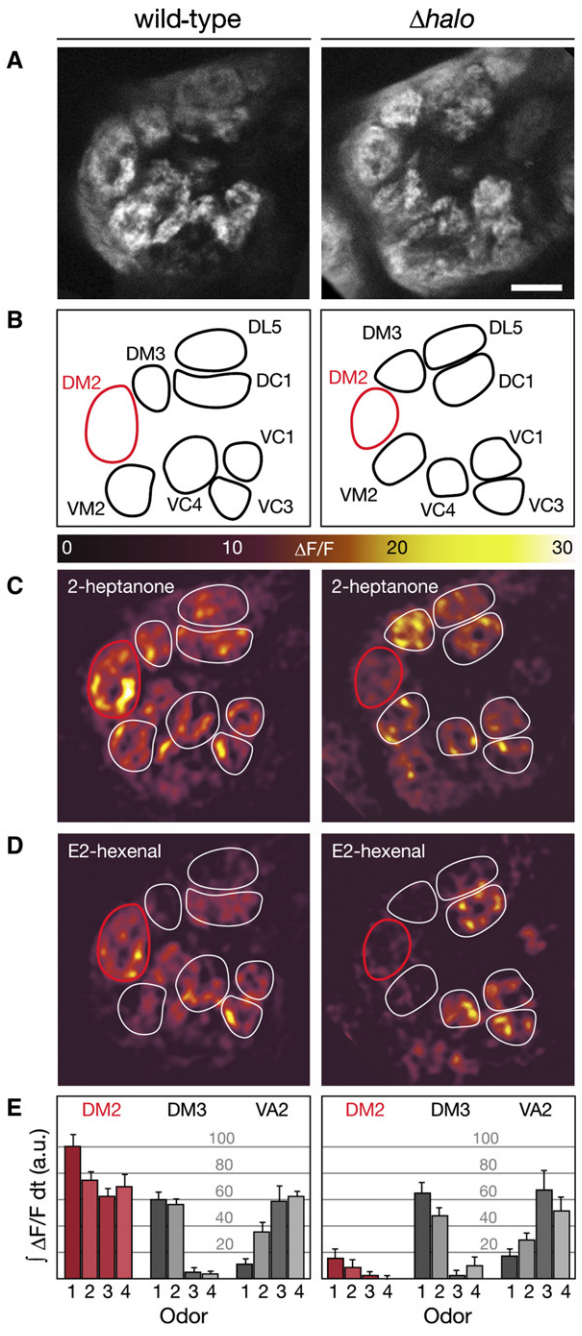

Figure 1. ORN Responses in Wild-Type and *Δhalo* Flies

ORN responses of wild-type (left column) or *Δhalo* flies (right column) carrying *Or83b-GAL4:UAS-spH* transgenes were stimulated with 2 s pulses of pure odors, at a concentration of 0.1% saturated vapor, and recorded by 2PLSM.

(A) Prestimulus images show spH-positive projections of ORNs to the antennal lobe. Scale bar, 10 μm.

(B) Anatomical maps of target glomeruli receiving ORN projections. The DM2 glomerulus, which is innervated by ab3A neurons, is outlined in red. In *Δhalo* flies, the genes encoding odorant receptors Or22a and Or22b are deleted from ab3A neurons.

(C) Functional maps of ORN responses to 0.1% 2-heptanone in wild-type (left) and *Δhalo* flies (right). The maps are pseudocolored according to the look-up table on top. Note the severe response attenuation in *Δhalo* DM2.

(D) Functional maps of ORN responses to 0.1% E2-hexenal in wild-type (left) and *Δhalo* flies (right). The maps are pseudocolored according to the look-up table on top. Note the selective loss of odor responsiveness in *Δhalo* DM2.

(E) Integrated fluorescence (area under the ΔF/F curve) of glomeruli DM2, DM3, or VA2 in wild-type (left) and *Δhalo* flies (right) carrying *Or22a-GAL4:UAS-spH, Or47a-GAL4:UAS-spH,* or *Or92a-GAL4:UAS-spH* transgenes, respectively. Note that only a single glomerulus in each antennal lobe receives spH-positive ORN projections in these experiments. ORN responses were stimulated with 2 s pulses of 2-heptanone (odor 1), ethyl acetate (odor 2), E2-hexenal (odor 3), or γ-valerolactone (odor 4) at concentrations of 0.1% saturated vapor. Integrated fluorescence signals are normalized to the response of wild-type ab3A neurons to 2-heptanone (i.e., the wild-type DM2 response to odor 1); data are displayed as means ± SEM (n = 6 individuals).

ORNs and PNs innervating a single glomerulus, DM2, have painted a different picture of information flow in the antennal lobes (Wilson et al., 2004). PNs were found to exhibit broader odor-receptive fields than their known ORN afferents, suggesting a convergence of multiple inputs. The nature of these inputs, the rules according to which they are combined, and the consequences for olfactory coding are not currently understood.

To begin to address these problems, we have selectively eliminated all monosynaptic ORN input to the DM2 glomerulus and examined if PNs innervating this glomerulus remain responsive to odors. A loss of PN responses under these conditions would demonstrate that PNs are driven exclusively by ORN afferents immediately presynaptic to them. ORN inputs to other glomeruli may modulate PN activity indirectly (for example, via inhibition) but would be unable to excite it. The persistence of PN responses in the absence of direct ORN input, on the other hand, would indicate that circuits in the antennal lobes redistribute ORN activity across the PN population. The question then arises how these circuits are configured and what purpose they serve in the detection and discrimination of odors.

RESULTS

PN Responses in the Absence of Monosynaptic Sensory Input

Comprehensive maps of odorant receptor expression and glomerular targeting in *Drosophila* (Couto et al., 2005; Fishilevich and Vosshall, 2005) indicate that the DM2 glomerulus receives its only monosynaptic sensory input from ab3A ORNs, which coexpress receptors Or22a, Or22b, and Or83b (Dobritsa et al., 2003; Larsson et al., 2004; Neuhaus et al., 2005). A synthetic deletion of ~100 kb in cytogenetic region 22A, termed *Δhalo*, removes the genes encoding Or22a and Or22b and virtually silences the ab3A neurons without altering their axonal projections (Dobritsa et al., 2003; below).

To verify the loss of odor responses in receptor-deficient ab3A neurons, the genetically encoded sensor of neurotransmitter release, spH (Miesenböck et al., 1998), was

expressed under the control of the *Or83b* promoter (Ng et al., 2002) in a large fraction of ORNs (Figures 1A and 1B). Odor-evoked fluorescence changes due to synaptic transmission in the antennal lobes were recorded by two-photon laser-scanning microscopy (2PLSM) (Ng et al., 2002; Roorda et al., 2004). Low concentrations of monomolecular test odorants (0.1% saturated vapor, corresponding to 0.62–35.45 ppm of isobutylene; see Experimental Procedures) elicited distributed patterns of ORN activity in wild-type and *Δhalo* flies (Figures 1C and 1D). Figure 1E quantifies the responses of three classes of ORNs (expressing Or22a/b, Or47a, and Or92a and targeting glomeruli DM2, DM3, and VA2, respectively) to four odors. The *Δhalo* deletion selectively impaired the function of ORNs projecting to DM2 (Figures 1C–1E, 2A, and 2B): it abolished responses to E2-hexenal and γ-valerolactone and severely reduced sensitivity to ethyl acetate and 2-heptanone.

The small residual signal registering upon stimulation with ethyl acetate and 2-heptanone reflects genuine ab3A activity rather than cryptic ORN inputs or fluorescence bleed-through from adjacent glomeruli, as fluorescence changes of equal magnitude were detected in *Δhalo; Or22a-GAL4:UAS-spH* flies, in which ORNs projecting to DM2 are the only spH-expressing cells (Figure 1E). Small residual odor responses of receptor-deficient ab3A neurons have also been documented electrophysiologically (Dobritsa et al., 2003). At concentrations comparable to those used in our experiments, some odors, such as 2-heptanone, elicit small firing rate increases from ~1 spike/s at baseline to ~18 spikes/s at peak in *Δhalo* mutants, as compared to increases from ~6 to >50 spikes/s in wild-type animals (Dobritsa et al., 2003; Hallem et al., 2004; Hallem and Carlson, 2006). Although the mechanism responsible for the residual odor responses of receptor-deficient ORNs is unclear, our ability to record this activity demonstrates that spH possesses adequate sensitivity to detect even small numbers of action potentials and confirms that 2PLSM provides sufficient spatial resolution to assign signals unambiguously to individual glomeruli.

To test whether DM2 PNs responded to odors in the verified absence of direct ORN input, we constructed flies that carried the *Δhalo* deletion, an *Or22a-dsRed* transgene to place an identifying label into DM2, and *GH146-GAL4:UAS-spH* transgenes to express spH in ~60% of PNs (Stocker et al., 1997). Glomerulus DM2 was identified visually, and responses of dendritic PN synapses to a panel of odorants, delivered at a concentration of 0.1% saturated vapor, were measured by 2PLSM (Ng et al., 2002). E2-hexenal, γ-valerolactone, ethyl acetate, and 2-heptanone all elicited robust synaptic activity in DM2 PNs (Figures 2 and 3). In contrast to the complete loss or severe reduction of ab3A ORN responses to these odors (Figures 1C–1E and 2B), DM2 PN response amplitudes were only moderately attenuated; they reached 32%–93% of wild-type levels (compare Figures 2A and 2B). This striking difference in the severity of *Δhalo*'s effects on ORNs and PNs can be understood if PNs pool direct and indirect inputs

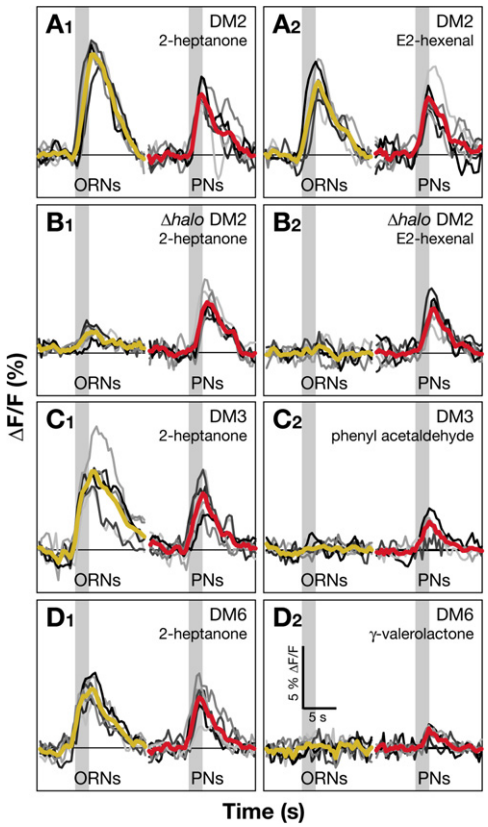

Figure 2. Comparison of ORN and PN Responses

(A–D) SpH was expressed in ORNs or PNs of wild-type (A, C, and D) or *Δhalo* (B) flies carrying *Or83b-GAL4:UAS-spH* or *GH146-GAL4:UAS-spH* transgenes, respectively. Responses were stimulated with 2 s pulses of pure odors, at a concentration of 0.1% saturated vapor, and recorded by 2PLSM. Background-normalized fluorescence (ΔF/F) of DM2 (A and B), DM3 (C), and DM6 (D) is plotted as a function of time. Individual (gray traces) and averaged odor responses (n = 4–6 individuals; ORNs in yellow and PNs in red) are shown; periods of odor application are indicated by gray-shaded backgrounds.

from multiple sources; excitatory drive from secondary inputs could then compensate, at least in part, for inactivity of the monosynaptic ORN afferent.

A potential caveat is that this conclusion is based on the analysis of a mutant, which might distort normal physiology. The chronic inactivation of ab3A ORNs in *Δhalo* animals might permit noncognate ORNs to invade the functionally vacant DM2 territory. If this were the case, the odor responses of DM2 PNs in *Δhalo* flies would reflect aberrant sensory innervation and, as such, a pathology particular to the mutant. To guard against such a misinterpretation of the *Δhalo* phenotype, we selectively ablated the ab3A neurons by expressing the cell-death gene *reaper* from the *Or22a* promoter (White et al., 1996; Dobritsa et al., 2003). Surviving ORN projections to the antennal lobe, which were labeled via a broadly expressed *Or83b-spH* transgene, were visualized by confocal microscopy. Optical sections through the antennal lobes

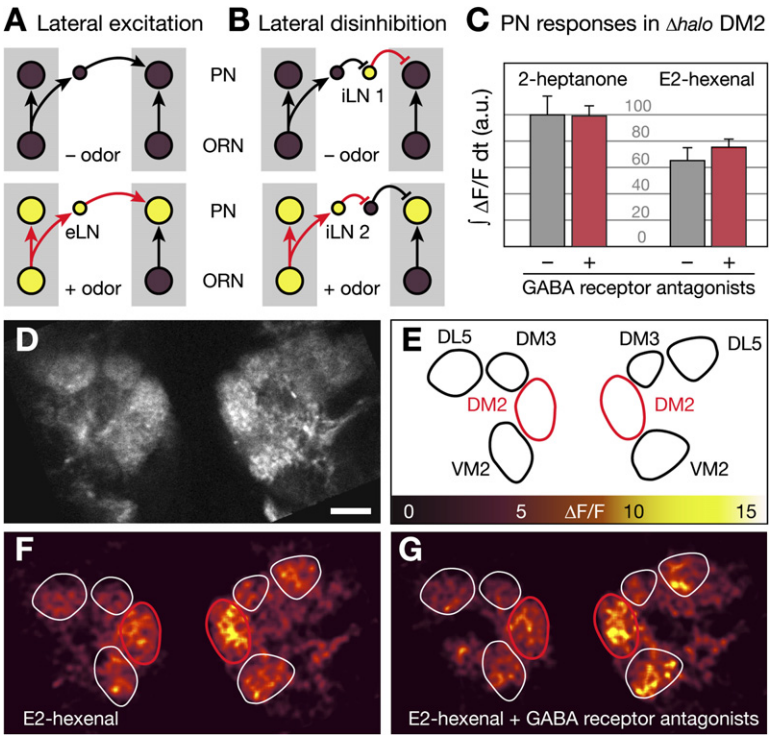

Figure 3. Lateral Excitation Versus Lateral Disinhibition of PNs

(A and B) Hypothetical circuits mediating lateral excitation (A) or lateral disinhibition (B) of PNs. Two glomerular channels are represented as gray-shaded rectangles. Each channel consists of a monosynaptic connection between ORNs and PNs, which are both symbolized by large circles. Small circles outside the glomerular channels represent LNs. Diagrams on top depict circuit states in the absence of odor; diagrams at the bottom show the consequences of activating ORNs feeding into the glomerular channel on the left. Inactive neuronal elements are colored in brown and active elements in yellow. Inactive synaptic connections are represented as black arrows and active connections as red arrows; excitation and inhibition symbols indicate the sign of each synapse. In lateral excitation (A), an excitatory LN (eLN) forms an interglomerular connection between an ORN in the glomerular channel on the left and a PN in the glomerular channel on the right. In lateral disinhibition (B), the interglomerular connection consists of two inhibitory LNs in series. In the absence of odor, a tonically active inhibitory LN (iLN 1) suppresses spontaneous PN activity in the glomerular channel on the right. Odor-evoked, phasic inhibition of iLN 1 by a second inhibitory LN (iLN 2) allows the PN on the right to escape from tonic inhibition.

(C) Integrated fluorescence (area under the ΔF/F curve) of glomerulus DM2 in *Δhalo* flies carrying *GH146-GAL4*:*UAS-spH* transgenes, in the presence and absence of 250 μM picrotoxin and 50 μM CGP54626. PN responses were stimulated with 2 s pulses of 0.1% 2-heptanone or 0.1% E2-hexenal. Integrated fluorescence signals are normalized to the response to 2-heptanone in the absence of GABA receptor antagonists; data are displayed as means ± SEM (n = 8 and 9 individuals, respectively, in the absence and presence of drug).

(D) Prestimulus image shows spH-positive PN synapses in the antennal lobes. Scale bar, 10 μm.

(E) Anatomical map of glomeruli innervated by PNs. The DM2 glomeruli are outlined in red.

(F) Functional map of PN responses to 0.1% E2-hexenal in a *Δhalo* fly. The map is pseudocolored according to the look-up table on top.

(G) Functional map of PN responses to 0.1% E2-hexenal in a *Δhalo* fly, in the presence of 250 μM picrotoxin and 50 μM CGP54626. The map is pseudocolored according to the look-up table on top.

revealed, at the location of the DM2 glomerulus, a sharply delineated cavity devoid of fluorescence (Figure S1): even a physically deafferented DM2 glomerulus did not attract ectopic ORN innervation, in accord with recent observations by others (Berdnik et al., 2006).

A second concern is that DM2 might represent a special case of a glomerulus with multiple inputs. To establish the generality and physiological relevance of our observations, we examined two additional glomeruli, DM3 and DM6, in wild-type flies. Consistent with a role for secondary inputs in normal physiology, PN responses could be stimulated in either glomerulus with odors that failed to activate its monosynaptic ORN afferent (Figures 2C and 2D).

Lateral Excitation Versus Lateral Disinhibition of PNs

What is the mechanism that allows PNs to respond to odors in the absence of monosynaptic ORN input? While electrical coupling (Schoppa and Westbrook, 2002) or neurotransmitter spillover (Isaacson, 1999) can provide means of local cell-to-cell communication within a glomerulus, long-range signaling between neurons in different glomeruli is likely to require chemical synaptic connections. From first principles, the logic of circuits transmitting excitatory signals from ORNs targeting one glomerulus to PNs innervating another must conform to one of two basic schemes (Figures 3A and 3B). (More elaborate anatomical layouts are conceivable, but these can always be reduced to logical equivalents of one or the other of the basic circuits in Figure 3.)

The first arrangement would result in direct "lateral excitation" of PNs, i.e., involve the interglomerular transmission of ORN inputs by excitatory local neurons (LNs) (Figure 3A). This scheme is speculative, as there is currently no evidence that the key elements required to build this type of circuit—excitatory LNs—are present within the antennal lobe.

The second synaptic arrangement would redistribute excitation indirectly via "lateral disinhibition" of PNs, i.e., through the odor-evoked release of PNs from tonic inhibition (Figure 3B). This arrangement seems anatomically plausible, as the antennal lobe is indeed densely innervated by inhibitory, GABAergic interneurons with multiglomerular processes (Stocker et al., 1990; Ng et al., 2002; Wilson et al., 2004; Wilson and Laurent, 2005). However, in

flies there is evidence neither for tonic inhibition of PNs by inhibitory LNs nor for the serial inhibitory connections that would be required to implement disinhibition (Figure 3B).

To distinguish between these mechanisms, we tested a critical prediction of lateral disinhibition. If activity is indeed relayed between glomeruli via inhibitory synapses, then blocking GABA receptors should eliminate all interglomerular communication. PNs lacking a direct ORN afferent should then be disconnected from sensory input and become unresponsive to odors. We generated such a situation experimentally by treating *Δhalo* flies (which lack a functional ORN afferent to DM2) with a cocktail of $GABA_A$ and $GABA_B$ receptor antagonists (250 μM picrotoxin and 50 μM CGP54626; Wilson and Laurent, 2005). Blocking GABA receptors caused a modest generalized increase in PN response amplitudes (from 4.02 ± 1.57 to 4.73 ± 1.77% ΔF/F, mean ± standard deviation (SD), n = 84 glomerulus-odor pairings; $p < 0.0005$, Wilcoxon signed rank test). The odor responses of DM2 PNs in *Δhalo* animals also persisted slightly enhanced or undiminished, in direct contradiction to the predictions of lateral disinhibition (Figure 3C; also, compare Figures 3F and 3G). Inhibitory synapses are thus not the main mode of communication through which secondary inputs are relayed among glomeruli.

A New Class of Cholinergic Local Neurons in the Antennal Lobes: Conductors of Lateral Excitation?

The vigorous odor responses of PNs in the simultaneous absence of monosynaptic ORN input and inhibitory synaptic transmission demand, by elimination, that excitatory channels for lateral communication among glomeruli exist. No class of neurons that could fulfill this role, however, has been identified: in the antennal lobes of flies, all excitatory synapses are thought to arise from the uniglomerular arborizations of ORNs and PNs; multiglomerular neurons are generally thought to be inhibitory.

In an effort to reconcile anatomy and function, we searched for excitatory neurons that could relay sensory input from ORNs targeting one glomerulus to PNs sampling another. Our search was based on the following two assumptions. First, candidate neurons mediating lateral excitation are local neurons lacking projections outside the antennal lobe. Second, these neurons signal through acetylcholine, which serves as the predominant excitatory neurotransmitter in the *Drosophila* CNS (Buchner, 1991); they will therefore express the biosynthetic enzyme choline acetyltransferase (ChAT). Our search accordingly centered on a set of enhancer-trap lines that allowed us to mark different, but perhaps overlapping, populations of LNs with membrane bound mCD8-GFP fusion proteins. Within these populations of fluorescently labeled LNs, we sought to identify cholinergic members by staining with an antibody against ChAT (Takagawa and Salvaterra, 1996). Parallel samples were labeled with an antibody against GABA to take advantage of a simple, direct, and independent crosscheck for ascertaining the sensitivity and specificity of detection: because neurons secreting excitatory and inhibitory neurotransmitter are expected to represent distinct populations, any enhancer-trap line containing ChAT-positive cells should show a commensurate reduction in the count of GABA-positive cells and vice versa.

Four enhancer-trap lines driving mCD8-GFP expression in LNs were analyzed. The enhancer elements of lines *KL78-GAL4* and *KL107-GAL4* are active in ~5 and 50 LNs, respectively; line *KL107-GAL4* also runs in ORNs projecting to nine glomeruli, in several PNs of the ventral cluster, and in some mushroom-body Kenyon cells (KCs). Line *189Y* is expressed in ~15 LNs of the antennal lobe, in a fraction of KCs, and in several neurons of the ellipsoid body. The line termed *krasavietz-GAL4* marks a dozen or so LNs in the antennal lobe and many KCs in the mushroom body (Dubnau et al., 2003).

Results of these analyses are illustrated in Figure 4 and summarized in Table S1. Of the four experimental enhancer-trap lines, two (*KL78-GAL4* and *189Y*) ran overwhelmingly if not entirely in GABAergic cells (not shown). Two other lines (*krasavietz-GAL4* and *KL107-GAL4*) labeled mixtures of GABAergic and cholinergic neurons in slightly different ratios. The fractions of cholinergic neurons in the GFP-expressing LN populations were substantial at 71% and 63% in *KL107-GAL4* and *krasavietz-GAL4*, respectively (Table S1).

The immunochemical procedures were validated with the help of two well-characterized control lines, *GH146-GAL4* and *GH298-GAL4*, which exhibit considerable specificity for cholinergic PNs and GABAergic LNs, respectively (Stocker et al., 1997). In *GH146-GAL4:UAS-mCD8-GFP* animals, ChAT-positive neurons accounted for 94% of all GFP-positive neurons, whereas in *GH298-GAL4:UAS-mCD8-GFP* animals, a majority of 81% of all GFP-positive neurons were GABA positive. GABAergic and cholinergic cells together made up close to 100% of all mCD8-GFP-expressing antennal lobe cells in each of the four enhancer-trap lines studied in detail, attesting to the completeness and specificity of our transmitter-phenotype assignments (Table S1).

Because *KL107-GAL4* labels two classes of cholinergic neurons innervating the antennal lobes (excitatory LNs plus a fraction of ORNs), only the *krasavietz-GAL4* driver, which runs exclusively in LNs, was used for the further characterization of excitatory LNs. An independent estimate of the number of excitatory and inhibitory LNs labeled by this driver was derived by comparing signals from *UAS-mCD8-GFP* and *UAS-spH* transgenes with dsRed expression from the *ChAT* promoter (Kitamoto et al., 1992). Confocal microscopy of reporter protein fluorescence revealed a smaller number of GFP-positive cells than antibody staining (10–12 versus ~15 cells; Table S2) and indicated large and systematic cell-to-cell variations in GFP-expression levels: 8–11 large, brightly fluorescent neurons extending a visible process into the lobe were identified as cholinergic by the presence of dsRed, whereas one or two smaller cells lacked dsRed and showed very faint GFP signals (Figure 7A, Movie S1, and Table S2). Taken together, these

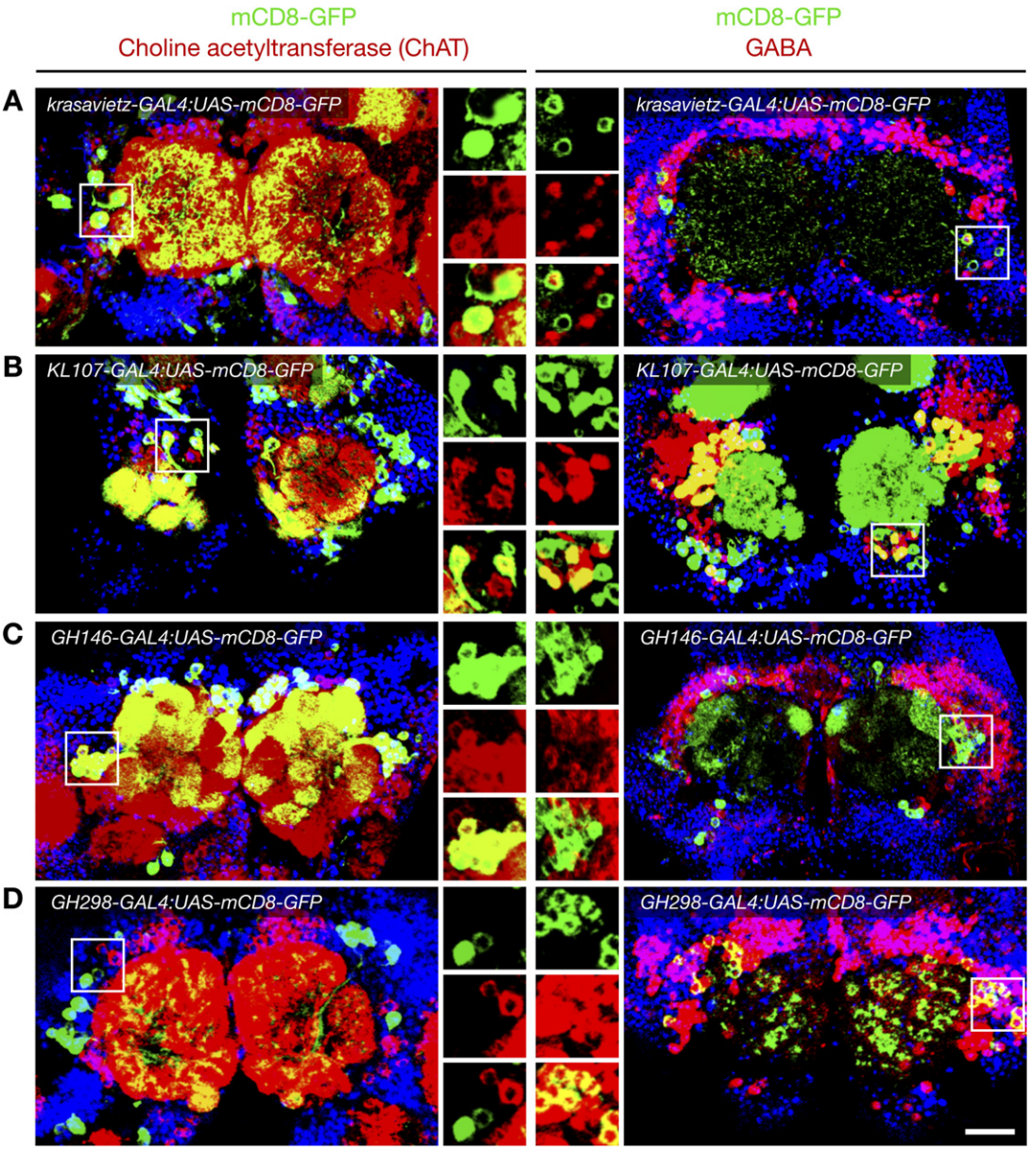

Figure 4. Cholinergic LNs of the Antennal Lobes

Dissected fly brains were immunolabeled with antibodies against GFP and ChAT (left column) or against GFP and GABA (right column) and counterstained with DAPI (blue). Maximum intensity projections of three to seven confocal sections through the antennal lobes, acquired at an axial spacing of 1 μm, are displayed. Single- and dual-channel fluorescence images of boxed areas are reproduced at higher magnification near the center of the figure (GFP in green; ChAT or GABA in red). Scale bar, 20 μm.

(A) The GFP-labeled cell population of flies carrying *krasavietz-GAL4:UAS-mCD8-GFP* transgenes consists mostly of cholinergic neurons.

(B) The GFP-labeled cell population of flies carrying *KL107-GAL4:UAS-mCD8-GFP* transgenes consists mostly of cholinergic neurons.

(C) The GFP-labeled cell population of flies carrying *GH146-GAL4:UAS-mCD8-GFP* transgenes consists mostly of cholinergic neurons.

(D) The GFP-labeled cell population of flies carrying *GH298-GAL4:UAS-mCD8-GFP* transgenes consists mostly of GABAergic neurons.

numbers suggest that the enhancer element trapped in the *krasavietz-GAL4* line is so weakly active in GABAergic LNs that detection of its activity requires signal amplification by indirect immunostaining. The differential expression of the enhancer in cholinergic and GABAergic LNs is a fortunate property, as it will allow us to image spH signals from excitatory LNs virtually free of contamination (Figure 7).

Innervation of the antennal lobes by cholinergic LNs was demonstrated directly by immunoelectron microscopy. Cryosections through the microdissected antennal lobes of flies carrying *krasavietz-GAL4:UAS-spH* transgenes

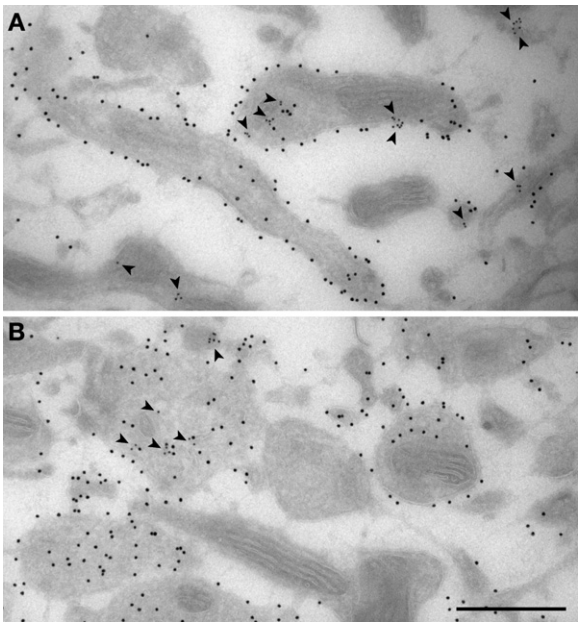

Figure 5. Immunogold Localization of ChAT to LN Processes in the Antennal Lobes

Cryosections through the antennal lobes of flies carrying *krasavietz-GAL4:UAS-spH* transgenes were double-labeled with antibodies against GFP (large gold) and ChAT (small gold; arrowheads). Staining with large gold particles identifies a fraction of profiles as spH-positive LNs. Consistent with the membrane localization and transmembrane topology of spH, the large gold particles decorate the extracellular face of the plasma membrane and the lumenal side of intracellular vesicles. Some LN profiles are double-labeled with small gold particles (arrowheads), which mark the locations of antibodies directed against ChAT (center in A; center left in B). The images also contain examples of unlabeled profiles (e.g., center in B) and of profiles single-labeled with small gold particles (lower left and upper right in A). Scale bar, 500 nm.

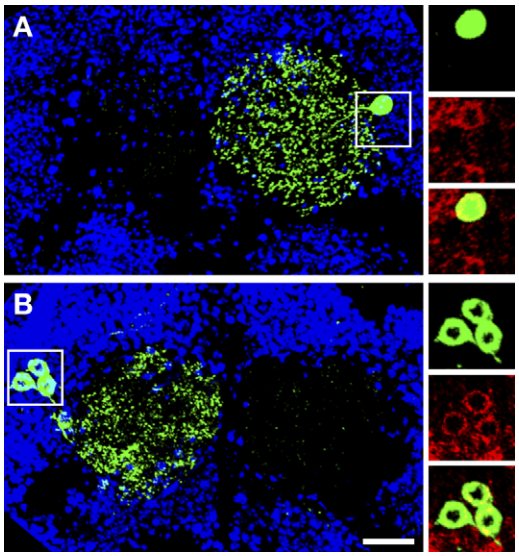

Figure 6. Dendritic Arbors of Cholinergic LNs Revealed by Clonal Analysis

Dissected fly brains were immunolabeled with antibodies against GFP (green) and ChAT (red) and counterstained with DAPI (blue). Maximum-intensity projections of 23–27 confocal sections through the antennal lobes, acquired at an axial spacing of 1 μm, are displayed. Single- and dual-channel fluorescence images of boxed areas are reproduced at higher magnification on the right (GFP in green; ChAT in red). Higher-magnification images are maximum-intensity projections of three to five confocal sections acquired at an axial spacing of 1 μm. Scale bar, 20 μm.

(A) Expression of a *UAS-spH* transgene under the control of the *krasavietz-GAL4* driver was induced in a single cholinergic LN by mitotic recombination during the first larval instar stage.

(B) Expression of a *UAS-spH* transgene under the control of the *krasavietz-GAL4* driver was induced in a cholinergic neuroblast clone by mitotic recombination during the first 7 hr of larval life.

were immunolabeled with antibodies against GFP and ChAT. In qualitative agreement with our light microscopic observations of ChAT-positive LN somata, 23% of the GFP-positive processes extended into the antennal lobe neuropil were also immunopositive for ChAT (Figure 5; n = 562 profiles in 70 randomly selected fields at a magnification of 26,500×; see Experimental Procedures). The relatively low percentage of ChAT-positive processes reflects the difficulty of preserving, under the harsh fixation conditions required for electron microscopy, the single epitope recognized by the monoclonal anti-ChAT antibody (Takagawa and Salvaterra, 1996).

Multiglomerular Arborizations of Excitatory LNs

Conductors of lateral excitation are expected anatomically to bridge between multiple glomeruli. To determine whether cholinergic LNs exhibited multiglomerular branching patterns, mosaic analysis with a repressible cell marker (MARCM) was performed to highlight single neurons or small neuroblast clones. Clonal analysis circumvented the difficulty of tracing individual neurites in populations of labeled cells (Lee and Luo, 1999; Jefferis et al., 2001). Briefly, the *krasavietz-GAL4* induced transcription of a *UAS-spH* transgene was placed under the control of a ubiquitously expressed, dominant GAL80 repressor. The repressor was subsequently removed in individual neuroblasts or neurons by inducing mitotic recombination (via the expression of FLP recombinase from a heat-shock promoter) at specific times during development.

A series of timed recombination events during the first 6 days of larval life, followed by immunostaining of 508 adult brains with anti-ChAT antibodies, allowed us to visualize individual LNs, determine their ChAT content, and delineate their branching patterns in the antennal lobes. Single cholinergic neurons (Figure 6A) and small neuroblast clones of two to four cells (Figure 6B) were seen most frequently when mitotic recombination took place during the first instar stage. Like the previously characterized GABAergic LNs (Stocker et al., 1990; Ng et al., 2002; Wilson et al., 2004; Wilson and Laurent, 2005), all cholinergic LNs we observed (n = 25) were commissure and axonless cells that extended a single dendritic trunk into the

center of one antennal lobe. There, the process arborized into numerous branches terminating in most, if not all, glomeruli (Figure 6).

Odor Responses of Excitatory LNs

Two separate estimates of the ratio of excitatory to inhibitory neurons labeled by the *krasavietz-GAL4* driver agree that cholinergic LNs predominate with a share of 63%–87% of all genetically marked cells (Tables S1 and S2 and Movie S1). If expression levels are taken into account, the balance tips fully in favor of excitatory neurons, as the *krasavietz-GAL4* enhancer shows only weak activity in GABAergic LNs: signal amplification is generally required to detect transgene expression in these cells. Cholinergic LNs, then, produce the overwhelming majority of spH in the antennal lobes of *krasavietz-GAL4:UAS-spH* flies (>95%; Figure 7A and Movie S1), permitting us to view odor-evoked fluorescence changes as an acceptably pure measure of the activity of these neurons.

All odors tested at a concentration of 0.1% saturated vapor activated LN synapses throughout the antennal lobes (Figure 7C). Because odors are potent agonists on some odorant receptors but not on others, ORN activity maps display the typical patchwork of active and inactive glomeruli (Figures 1C and 1D). Very little odor-specific spatial structure, in contrast, was evident in excitatory LN activity patterns, whose response amplitudes appeared nearly uniform across glomeruli (Figure 7C). Odors thus elicit two qualitatively different types of excitatory synaptic activity in the antennal lobes: focal, glomerulus- and odor-specific ORN signals, and a diffuse background of excitatory LN activity. The receptive properties of PNs suggest that these neurons combine synaptic inputs from both of these sources.

DISCUSSION

The Circuit Diagram of the Antennal Lobe

Functional and anatomical studies have revealed that the circuitry of the antennal lobe contains, in addition to ORNs, PNs, and inhibitory LNs, a fourth neuronal element: excitatory LNs. These intrinsic antennal lobe neurons synthesize the neurotransmitter acetylcholine (Figures 4–7A), respond to odors (Figure 7), and are anatomically configured to bridge between many glomeruli (Figure 6). The discovery of excitatory LNs provides a simple anatomical basis for several findings that have been difficult to accommodate by the "standard model" of olfactory processing. According to this model, the antennal lobe is organized as a bundle of labeled ORN-PN lines, which exchange information exclusively through inhibitory lateral interconnections.

The first hint that the standard model might be incomplete came from electrophysiological work, which indicated that some PNs possess broader odor-receptive fields than the ORNs immediately presynaptic to them (Wilson et al., 2004). This suggested that PNs can pool

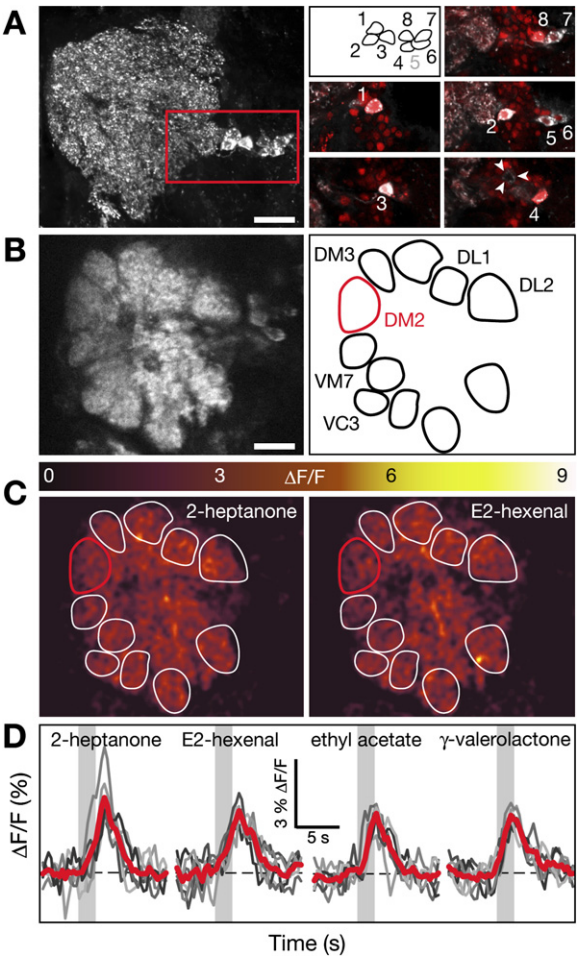

Figure 7. Optical Imaging of Excitatory LN Responses

(A) Maximum-intensity projection of 40 confocal sections through the antennal lobe of a fly carrying *krasavietz-GAL4*, *UAS-mCD8-GFP*, *UAS-spH,* and *Cha-dsRed* transgenes, acquired at an axial spacing of 1 μm. Native GFP fluorescence reveals dense innervation of all glomeruli from a laterally situated cluster of 8 LNs (left, cell 5 obscured). Individual confocal sections through the LN cluster demonstrate coexpression of dsRed in all eight neurons, identifying them as cholinergic (right). One additional, very weakly fluorescent cell body is dsRed-negative (arrowheads) and thus, presumably, GABAergic. Scale bar, 10 μm. A high-resolution view through the stack of confocal sections is available online (Movie S1).

(B) Prestimulus 2PLSM image of a fly carrying *krasavietz-GAL4:UAS-spH* transgenes shows spH-positive LN synapses in glomeruli of the antennal lobe and cell-membrane staining in a laterally situated cluster of LN somata (left). Scale bar, 10 μm. An anatomical map identifies some of the glomeruli innervated by LNs (right). The DM2 glomerulus is outlined in red.

(C) Functional maps of LN responses to 0.1% 2-heptanone (left) and 0.1% E2-hexenal (right) in a wild-type fly carrying *krasavietz-GAL4:UAS-spH* transgenes. The maps are pseudocolored according to the look-up table on top.

(D) Background-normalized fluorescence (ΔF/F) of DM2 as a function of time in wild-type flies carrying *krasavietz-GAL4:UAS-spH* transgenes. Individual (gray traces) and averaged responses (n = 6 individuals; red traces) to 2 s odor pulses are shown; periods of odor application are indicated by gray-shaded backgrounds.

excitatory inputs from several, then unknown, sources. Second, we have shown here that the PNs innervating a particular glomerulus respond to odors even if an odorant-receptor deletion silences the only monosynaptic ORN afferent to this glomerulus (Figures 2 and 3). This establishes that a polysynaptic circuit within the antennal lobe, not the convergence of multiple ORN inputs onto the same glomerulus, is responsible for the broadening of PN-receptive fields. Third, we have demonstrated that the polysynaptic circuit consists of excitatory neurons, as it remains functional under conditions where inhibitory synaptic transmission is blocked (Figure 3C). The simplest circuit to account for these findings is shown in Figure 3A. ORNs projecting to one glomerulus are connected with the PNs sampling another via two excitatory synapses: one synapse from an ORN onto an excitatory LN and a second synapse from the excitatory LN onto a PN.

Although the circuit depicted in Figure 3A is consistent with all experimental facts, important details of its connectivity and function remain to be established. Because we may currently not be able to mark all excitatory LNs genetically, we do not know how many of them innervate the antennal lobes, and we cannot test their physiological and behavioral roles by manipulating their activity (Kitamoto, 2001; Lima and Miesenböck, 2005). We do not yet know if excitatory LNs are indeed postsynaptic to ORNs and presynaptic to PNs. If these synaptic connections are found as expected, it remains to be determined whether ORNs represent the sole sources of excitatory input to cholinergic LNs and whether PNs constitute their sole postsynaptic targets. It would seem likely that excitatory and inhibitory LNs communicate, but we have at present no knowledge of the extent and direction of their functional interconnections.

Functional Architecture in the Olfactory System

The observed increase in receptive range between ORNs and PNs prompted the formulation of an alternative to the labeled-line model of olfactory coding (Wilson et al., 2004). Rather than traversing the antennal lobes in dedicated channels segregated by receptor type, olfactory signals were proposed to undergo complex transformations that decorrelate the lobe's output from its input. Our findings raise a third possibility. While PNs clearly respond to a broader range of odors than their monosynaptic ORN afferents (Figure 2), the change in receptive field size could be the consequence of a simple neural operation: the addition of a positive offset to many or all glomerular channels, due to diffuse excitation of PNs by cholinergic LNs (Figure 7).

Previous optical recordings (Ng et al., 2002; Wang et al., 2003) succeeded in visualizing the activation of individual glomerular channels but not the background of lateral excitation on which these activity patterns are now seen to ride. The unambiguous detection of this excitatory background required several experimental refinements: an increase in spH signal strength (by expressing multiple copies of a *UAS-spH* transgene), a reduction in background fluorescence (by imaging young adults and minimizing the release of eye pigment during dissection), and a reduction in photon-shot noise (by lowering the sampling rate and, in some instances [e.g., Figures 2C and 2D], averaging trials). Stimulation with low concentrations of monomolecular odorants in place of odor blends led to sparser ORN-input patterns that could be contrasted more clearly with the broadened PN responses they elicit. And, the *Δhalo* deletion provided an exceptionally favorable case for detecting PN excitation independent of monosynaptic ORN input (Figure 2).

The functional consequences of adding an offset to PN signals are best appreciated from the perspective of the two groups of neurons onto which PN activity is projected: the KCs of the mushroom bodies and the principal neurons of the lateral protocerebra. Of these two groups of third-order olfactory neurons, we consider only KCs, because insufficient anatomical and physiological information currently exists about lateral protocerebral neurons. In all insects studied to date, KCs outnumber PNs by more than a dozen-fold, yet each KC maintains synaptic contact with a large fraction of the PN population (~50% of all PNs in locusts; Mazor and Laurent, 2005). Despite this massive convergence of PN input, KCs encode olfactory information in an ultrasparse manner: basal KC activity is virtually nil, and odor applications elicit no more than one or two spikes in a handful of cells (Perez-Orive et al., 2002; Wang et al., 2004). Complex, dense PN representations are thus transformed into canonical, sparse KC representations. The biophysical mechanism underlying this transformation is coincidence detection: KCs possess high action-potential thresholds and short integration time windows and thus require large numbers of near-simultaneous synaptic inputs to reach threshold (Laurent and Naraghi, 1994; Perez-Orive et al., 2002 and 2004).

Coincidence detection, however, works reliably over only a limited dynamic range. Above this range, where synaptic impulses are too numerous, detectors are triggered by chance coincidences and report spurious signals; below this range, synaptic impulses are too few to sum to threshold, and detection failures ensue. Because odors of different quality and intensity cause large variations in ORN-activity levels (Ng et al., 2002; Hallem and Carlson, 2006), KCs would face a serious problem of dynamic range if they were connected directly to raw sensory input. One solution to this problem is for the circuitry of the antennal lobes to maintain global activity levels within the proper input range of KCs. Consistent with such an adaptive role of the antennal lobes, average PN firing rates in locusts remain constant across multiple odors and 1000-fold changes in odorant concentration (Stopfer et al., 2003). Inhibitory LNs have been implicated theoretically (Borst, 1983) and experimentally (Wilson and Laurent, 2005) in decreasing PN firing rates at high odor concentrations. We propose that excitatory LNs play an analogous, but opposite, role at low odor concentrations, increasing and redistributing odor-evoked activity over a larger ensemble of PNs.

In many threshold systems, the injection of a judicious amount of background noise can benefit faint signals by boosting them above threshold (Movie S2) (Wiesenfeld and Moss, 1995; Gammaitoni et al., 1998). When the background activity level is optimal for a given signal intensity (hence the somewhat misleading term "stochastic resonance"), a nonlinear detector, such as a KC, can faithfully report on an otherwise undetectable signal. Theorists have invoked stochastic resonance as a general strategy of the nervous system to ensure the reliable transmission of information (Knight, 1972; Longtin et al., 1991; Stemmler et al., 1995), but empirically documented cases are few and limited to environmental effects on sensory transduction (Douglass et al., 1993; Levin and Miller, 1996). The antennal lobe, then, may provide one of the first illustrations of how the addition of background activity from an internal source (excitatory LN input to PNs) enhances the communication of a deterministic neuronal signal (ORN input to PNs) to a threshold detector (KCs) in a central circuit of the brain.

EXPERIMENTAL PROCEDURES

Fly Strains

To visualize synaptic activity, flies were equipped with two GAL4-responsive supercliptic spH (*UAS-spH*) transgenes (Miesenböck et al., 1998; Ng et al., 2002) in either wild-type or *Δhalo* backgrounds (Dobritsa et al., 2003). Strains for anatomical studies carried *UAS-mCD8-GFP* and/or *UAS-spH* transgenes, strains for cell-ablation experiments a *UAS-rpr* expression cassette (White et al., 1996; Dobritsa et al., 2003). Strains used in MARCM experiments are described below.

Transgene expression was activated in specific sets of olfactory neurons by crossing *UAS* responder strains to the appropriate *GAL4* driver lines. Broad expression in ORNs was enabled by strain *Or83b-GAL4* (Ng et al., 2002), selective expression in specific classes of ORNs by strains *Or22a-GAL4* (Dobritsa et al., 2003), *Or47a-GAL4* (Vosshall et al., 2000), and *Or92a-GAL4* (Komiyama et al., 2004). A majority of PNs were labeled by the enhancer-trap line *GH146-GAL4* (Stocker et al., 1997). Transgene expression in subsets of antennal lobe LNs was controlled by driver lines *GH298-GAL4* (Stocker et al., 1997), *KL78-GAL4*, *KL107-GAL4* (http://web.neurobio.arizona.edu/Flybrain/html/genes/enhancer/list.html), *189Y* (http://www.fly-trap.org), and *krasavietz-GAL4* (Dubnau et al., 2003). Where the expression of two transgenes in two distinct populations of neurons was required—i.e., in double-labeling and cell-ablation experiments—the expression of one transgene was controlled by direct fusion to a cell-type specific promoter (*Or22a-dsRed*, *Cha-dsRed*, and *Or83b-spH*), whereas the other relied on the *GAL4-UAS* system (*GH146-GAL4:UAS-spH*, *krasavietz-GAL4:UAS-mCD8-GFP*, and *OR22a-GAL4:UAS-rpr*). Direct promoter fusions included 7.087, 7.347, and 8.197 kb of sequence upstream of the translation-start codons of *Or83b* (Ng et al., 2002), *Cha* (Kitamoto et al., 1992), and *Or22a* (Dobritsa et al., 2003), respectively.

Functional Imaging

SpH signals emitted by ORNs, PNs, or LNs were imaged by 2PLSM (Ng et al., 2002; Roorda et al., 2004). The antennal lobes were viewed through an opening in the postoccipital plate of the head, which was superfused with a solution containing 5 mM Na-HEPES, pH 7.5, 115 mM NaCl, 5 mM KCl, 6 mM $CaCl_2$, 1 mM $MgCl_2$, 4 mM $NaHCO_3$, 5 mM trehalose, 10 mM glucose, and 65 mM sucrose. To block GABAergic synaptic transmission where indicated, 250 μM picrotoxin (Sigma) and 50 μM CGP54626 (Tocris) were added from 1000× stock solutions in DMSO (Wilson and Laurent, 2005).

Fluorescence was excited with 100 fs pulses of light centered at 910 nm (Tsunami Ti:sapphire oscillator with Millennia Xs pump laser; Spectra Physics). The laser beam was steered by an Oz scan engine (ThermoNORAN) with spatial and temporal dispersion corrective optics (Roorda et al., 2004) and focused by a 40x, 0.8 W Zeiss IR-Achroplan objective. Emitted photons were separated from excitation light by a series of dichromatic mirrors and dielectric and colored glass filters and detected by a photomultiplier tube (R3896; Hamamatsu Photonics) in whole-field mode. The 30 Hz video signal was digitized by a National Instruments PCI-1409 video-acquisition board and analyzed offline in MetaMorph 5.0 and Matlab 7.1. Images (600 × 480 pixels) were corrected for a smoothed Statistical Parametric Mapping (SPM) motion estimate (Friston et al., 1995) and normalized to a moving-average fluorescence background (Roorda et al., 2004). The displayed fluorescence traces represent 10-frame averages at an effective temporal resolution of 3 Hz. Pseudocolored activity maps were computed by subtracting a 50 frame (1.67 s) prestimulus average from a 50 frame (1.67 s) stimulus average containing the ΔF/F peak and convolving the difference image with a 15 × 15 pixel Gaussian kernel.

Odor-evoked synaptic release was stimulated by 2 s pulses of a panel of test odorants (Table S3). The pulses were generated by switching software-controlled solenoid valves (The Lee Company) to combine two mass flow-controlled gas streams (CMOSens PerformanceLine; Sensirion): a 450 ml/min carrier stream of filtered, humidified air and a 50 ml/min stimulus stream drawn through a gas washing tube filled with 5 ml of liquid odorant at 1:100 dilution (vol/vol) in paraffin oil. The nominal odor concentration at the outlet of the delivery tube was 0.1% saturated vapor; concentrations measured with a ppbRAE photoionization detector calibrated for isobutylene averaged 35,450 ± 9,474 parts per billion (ppb) for ethyl acetate, 5621 ± 1005 ppb for E2-hexenal, 621 ± 28 ppb for γ-valerolactone, and 7499 ± 853 ppb for 2-heptanone (means ± standard error of the mean [SEM] of triplicate measurements). Correcting for the known difference in ionization energy between ethyl acetate and isobutylene, the measured concentration of this odorant at a nominal concentration of 0.1% was 0.17% saturated vapor. Image acquisition and odor delivery were controlled by a virtual instrument written in LabVIEW 7.1.

Immunofluorescence Microscopy

Dissected fly brains were fixed in phosphate-buffered saline (PBS) containing 4% (vol/vol) paraformaldehyde plus 0.01% (vol/vol) Triton X-100 (PBS-T), permeabilized with 0.2% Triton X-100, and blocked in 0.5% (w/vol) BSA in PBS-T. To test for the presence of cholinergic and GABAergic LNs in populations of GFP-expressing neurons, parallel samples were double-labeled with mouse monoclonal antibody 4B1 against *Drosophila* ChAT (1:1,000; Takagawa and Salvaterra, 1996) and rabbit polyclonal antibodies against GFP (1:1,000), or with rabbit polyclonal antibodies against the neurotransmitter GABA (1:100; Sigma) and mouse monoclonal antibodies against GFP (1:100; Roche). Bound antibodies were detected with secondary AlexaFluor-488 and AlexaFluor-546 conjugates (Molecular Probes) at 1:500 dilution. Brains were mounted in VectaShield with DAPI (Vector Laboratories), and image stacks with an axial spacing of 1 μm were collected on a Zeiss LSM 510 confocal laser-scanning microscope. To estimate the percentages of ChAT or GABA-positive LNs, double-labeled somata located within a ~20 μm zone from the margin of the antennal lobe neuropil were counted. A positive score required colocalization of ChAT or GABA with GFP signals in a minimum of two adjacent focal planes.

Immunoelectron Microscopy

Microdissected antennal lobes were fixed in 4% paraformaldehyde in 0.25 M Na-HEPES, pH 7.4, for 1 hr, followed by overnight fixation in 8% paraformaldehyde at 4°C. Samples were stained by adding a few drops of a 1% (vol/vol) toluidine blue and 1% (w/vol) borate solution,

rinsed several times in PBS to remove excess stain, and embedded in 10% bovine gelatin (w/vol) in PBS. Blocks of gelatin containing single antennal lobes were infiltrated with 2.3 M sucrose in PBS and frozen in liquid nitrogen. Frozen 75 nm sections were cut on a Leica UltraCut ultramicrotome with a FCS cryoattachment at −108°C and collected on formvar- and carbon-coated nickel grids using a 1:1 mixture of 2% methyl cellulose and 2.3 M sucrose in PBS (Liou et al., 1996). After free aldehydes had been quenched with 0.1 M NH_4Cl, the grids were incubated in 1% fish skin gelatin (w/vol) in PBS (PBS-FSG), followed by sequential staining with mouse monoclonal anti-ChaT antibody 4B1 (1:100 to 1:1,000; Takagawa and Salvaterra, 1996), rabbit anti-mouse IgG (1:100; Cappel), and 10 nm Protein A-gold (Department of Cell Biology, Utrecht University) in PBS-FSG. After intermediate fixation (1% glutaraldehyde for 5 min) and quenching, the sections were exposed sequentially to rabbit anti-GFP antibody (1:100; Molecular Probes) and 15 nm Protein A-gold conjugate. The sections were then fixed with 1% glutaraldehyde, incubated with a mixture of 1.8% methyl cellulose and 0.5% uranyl acetate, air-dried, and visualized in a Tecnai 12 Biotwin electron microscope. For quantitation, 70 antennal lobe regions, each containing at least one labeled profile, were sampled at random at a magnification of 26,500×. A positive count required the presence of a minimum of three gold particles (or clusters of gold particles) per profile.

Clonal Analysis (MARCM)

Female *yw*, *hsFLP*; FRT^{G13}, *tubP-Gal80* flies were crossed to FRT^{G13}, *UAS-spH/CyO*; *krasavietz-GAL4*, *UAS-spH/TM3Tb* males. After appropriate aging, larval progeny were heat shocked for 1 hr at 37°C and allowed to develop for 2–4 days after eclosion (Lee and Luo, 1999). Adult male *hsFLP/Y*; FRT^{G13}, *tubP-Gal80*/FRT^{G13}, *UAS-spH*; *krasavietz-GAL4*, *UAS-spH*/+ flies were dissected and processed for immunofluorescence microscopy with anti-ChAT and anti-GFP antibodies, as described above.

Supplemental Data

Supplemental Data include one figure, three tables, and two movies and can be found with this article online at http://www.cell.com/cgi/content/full/128/3/601/DC1/.

ACKNOWLEDGMENTS

We are grateful to Dylan Clyne for odor-concentration measurements, to Robert Roorda for help with instrumentation, to Kim Zichichi for assistance with immunoelectron microscopy, to Elissa Hallem and John Carlson for sharing unpublished information, to Ajay Srivastava, Tatsushi Igaki, Laura Pedraza, and Tian Xu for access to their confocal microscope, and to Peter Takizawa and Graham Warren for comments on the manuscript. Paul Salvaterra donated antibodies; Douglas Armstrong, John Carlson, Liqun Luo, Reinhard Stocker, Klemens Störtkuhl, Tim Tully, and Leslie Vosshall provided fly strains. This work was supported by a grant from the NIH.

Received: May 30, 2006
Revised: September 5, 2006
Accepted: December 18, 2006
Published: February 8, 2007

REFERENCES

Berdnik, D., Chihara, T., Couto, A., and Luo, L. (2006). Wiring stability of the adult Drosophila olfactory circuit after lesion. J. Neurosci. *26*, 3367–3376.

Borst, A. (1983). Computation of olfactory signals in Drosophila melanogaster. J. Comp. Physiol. [A] *152*, 373–383.

Buchner, E. (1991). Genes expressed in the adult brain of Drosophila and effects of their mutations on behavior: a survey of transmitter- and second messenger-related genes. J. Neurogenet. *7*, 153–192.

Buck, L., and Axel, R. (1991). A novel multigene family may encode odorant receptors: a molecular basis for odor recognition. Cell *65*, 175–187.

Buonviso, N., Chaput, M.A., and Scott, J.W. (1991). Mitral cell-to-glomerulus connectivity: an HRP study of the orientation of mitral cell apical dendrites. J. Comp. Neurol. *307*, 57–64.

Clyne, P.J., Warr, C.G., Freeman, M.R., Lessing, D., Kim, J., and Carlson, J.R. (1999). A novel family of divergent seven-transmembrane proteins: candidate odorant receptors in Drosophila. Neuron *22*, 327–338.

Couto, A., Alenius, M., and Dickson, B.J. (2005). Molecular, anatomical, and functional organization of the Drosophila olfactory system. Curr. Biol. *15*, 1535–1547.

Dobritsa, A.A., van der Goes van Naters, W., Warr, C.G., Steinbrecht, R.A., and Carlson, J.R. (2003). Integrating the molecular and cellular basis of odor coding in the Drosophila antenna. Neuron *37*, 827–841.

Douglass, J.K., Wilkens, L., Pantazelou, E., and Moss, F. (1993). Noise enhancement of information-transfer in crayfish mechanoreceptors by stochastic resonance. Nature *365*, 337–340.

Dubnau, J., Chiang, A.S., Grady, L., Barditch, J., Gossweiler, S., McNeil, J., Smith, P., Buldoc, F., Scott, R., Certa, U., et al. (2003). The staufen/pumilio pathway is involved in Drosophila long-term memory. Curr. Biol. *13*, 286–296.

Fishilevich, E., and Vosshall, L.B. (2005). Genetic and functional subdivision of the Drosophila antennal lobe. Curr. Biol. *15*, 1548–1553.

Friston, K.J., Ashburner, J., Frith, C.D., Poline, J.B., Heather, J.D., and Frackowiak, R.S.J. (1995). Spatial registration and normalization of images. Hum. Brain Mapp. *2*, 165–189.

Gammaitoni, L., Hänggi, P., Jung, P., and Marchesoni, F. (1998). Stochastic resonance. Rev. Mod. Phys. *70*, 223–287.

Gao, Q., Yuan, B., and Chess, A. (2000). Convergent projections of Drosophila olfactory neurons to specific glomeruli in the antennal lobe. Nat. Neurosci. *3*, 780–785.

Hallem, E.A., and Carlson, J.R. (2006). Coding of odors by a receptor repertoire. Cell *125*, 143–160.

Hallem, E.A., Ho, M.G., and Carlson, J.R. (2004). The molecular basis of odor coding in the Drosophila antenna. Cell *117*, 965–979.

Isaacson, J.S. (1999). Glutamate spillover mediates excitatory transmission in the rat olfactory bulb. Neuron *23*, 377–384.

Jefferis, G.S.X.E., Marin, E., Stocker, R.F., and Luo, L. (2001). Target neuron prespecification in the olfactory map of Drosophila. Nature *414*, 204–208.

Kitamoto, T. (2001). Conditional modification of behavior in Drosophila by targeted expression of a temperature-sensitive shibire allele in defined neurons. J. Neurobiol. *47*, 81–92.

Kitamoto, T., Ikeda, K., and Salvaterra, P.M. (1992). Analysis of cis-regulatory elements in the 5′ flanking region of the Drosophila melanogaster choline acetyltransferase gene. J. Neurosci. *12*, 1628–1639.

Knight, B.W. (1972). Dynamics of encoding in a population of neurons. J. Gen. Physiol. *59*, 734–766.

Komiyama, T., Carlson, J.R., and Luo, L. (2004). Olfactory receptor neuron axon targeting: intrinsic transcriptional control and hierarchical interactions. Nat. Neurosci. *7*, 819–825.

Larsson, M.C., Domingos, A.I., Jones, W.D., Chiappe, M.E., Amrein, H., and Vosshall, L.B. (2004). Or83b encodes a broadly expressed odorant receptor essential for Drosophila olfaction. Neuron *43*, 703–714.

Laurent, G., and Naraghi, M. (1994). Odorant-induced oscillations in the mushroom bodies of the locust. J. Neurosci. *14*, 2993–3004.

Lee, T., and Luo, L. (1999). Mosaic analysis with a repressible cell marker for studies of gene function in neuronal morphogenesis. Neuron *22*, 451–461.

Levin, J.E., and Miller, J.P. (1996). Broadband neural encoding in the cricket cercal sensory system enhanced by stochastic resonance. Nature *380*, 165–168.

Lima, S.Q., and Miesenböck, G. (2005). Remote control of behavior through genetically targeted photostimulation of neurons. Cell *121*, 141–152.

Liou, W., Geuze, H.J., and Slot, J.W. (1996). Improving structural integrity of cryosections for immunogold labeling. Histochem. Cell Biol. *106*, 41–58.

Longtin, A., Bulsara, A., and Moss, F. (1991). Time-interval sequences in bistable systems and the noise-induced transmission of information by sensory neurons. Phys. Rev. Lett. *67*, 656–659.

Mazor, O., and Laurent, G. (2005). Transient dynamics versus fixed points in odor representations by locust antennal lobe projection neurons. Neuron *48*, 661–673.

Miesenböck, G., De Angelis, D.A., and Rothman, J.E. (1998). Visualizing secretion and synaptic transmission with pH-sensitive green fluorescent proteins. Nature *394*, 192–195.

Mombaerts, P., Wang, F., Dulac, C., Chao, S.K., Nemes, A., Mendelsohn, M., Edmondson, J., and Axel, R. (1996). Visualizing an olfactory sensory map. Cell *87*, 675–686.

Neuhaus, E.M., Gisselmann, G., Zhang, W., Dooley, R., Störtkuhl, K., and Hatt, H. (2005). Odorant receptor heterodimerization in the olfactory system of Drosophila melanogaster. Nat. Neurosci. *8*, 15–17.

Ng, M., Roorda, R.D., Lima, S.Q., Zemelman, B.V., Morcillo, P., and Miesenböck, G. (2002). Transmission of olfactory information between three populations of neurons in the antennal lobe of the fly. Neuron *36*, 463–474.

Perez-Orive, J., Mazor, O., Turner, G.C., Cassenaer, S., Wilson, R.I., and Laurent, G. (2002). Oscillations and sparsening of odor representations in the mushroom body. Science *297*, 359–365.

Perez-Orive, J., Bazhenov, M., and Laurent, G. (2004). Intrinsic and circuit properties favor coincidence detection for decoding oscillatory input. J. Neurosci. *24*, 6037–6047.

Ressler, K.J., Sullivan, S.L., and Buck, L.B. (1994). Information coding in the olfactory system: evidence for a stereotyped and highly organized epitope map in the olfactory bulb. Cell *79*, 1245–1255.

Roorda, R.D., Hohl, T.M., Toledo-Crow, R., and Miesenböck, G. (2004). Video-rate nonlinear microscopy of neuronal membrane dynamics with genetically encoded probes. J. Neurophysiol. *92*, 609–621.

Schoppa, N.E., and Westbrook, G.L. (2002). AMPA autoreceptors drive correlated spiking in olfactory bulb glomeruli. Nat. Neurosci. *5*, 1194–1202.

Stemmler, M., Usher, M., and Niebur, E. (1995). Lateral interactions in primary visual cortex: a model bridging physiology and psychophysics. Science *269*, 1877–1880.

Stocker, R.F., Heimbeck, G., Gendre, N., and de Belle, J.S. (1997). Neuroblast ablation in Drosophila P[GAL4] lines reveals origins of olfactory interneurons. J. Neurobiol. *32*, 443–456.

Stocker, R.F., Lienhard, M.C., Borst, A., and Fischbach, K.F. (1990). Neuronal architecture of the antennal lobe in Drosophila melanogaster. Cell Tissue Res. *262*, 9–34.

Stopfer, M., Jayaraman, V., and Laurent, G. (2003). Intensity versus identity coding in an olfactory system. Neuron *39*, 991–1004.

Takagawa, K., and Salvaterra, P. (1996). Analysis of choline acetyltransferase protein in temperature sensitive mutant flies using newly generated monoclonal antibody. Neurosci. Res. *24*, 237–243.

Vassar, R., Chao, S.K., Sitcheran, R., Nunez, J.M., Vosshall, L.B., and Axel, R. (1994). Topographic organization of sensory projections to the olfactory bulb. Cell *79*, 981–991.

Vosshall, L.B., Amrein, H., Morozov, P.S., Rzhetsky, A., and Axel, R. (1999). A spatial map of olfactory receptor expression in the Drosophila antenna. Cell *96*, 725–736.

Vosshall, L.B., Wong, A.M., and Axel, R. (2000). An olfactory sensory map in the fly brain. Cell *102*, 147–159.

Wang, J.W., Wong, A.M., Flores, J., Vosshall, L.B., and Axel, R. (2003). Two-photon calcium imaging reveals an odor-evoked map of activity in the fly brain. Cell *112*, 271–282.

Wang, Y., Guo, H.F., Pologruto, T.A., Hannan, F., Hakker, I., Svoboda, K., and Zhong, Y. (2004). Stereotyped odor-evoked activity in the mushroom body of Drosophila revealed by green fluorescent protein-based Ca2+ imaging. J. Neurosci. *24*, 6507–6514.

White, K., Tahaoglu, E., and Steller, H. (1996). Cell killing by the Drosophila gene reaper. Science *271*, 805–807.

Wiesenfeld, K., and Moss, F. (1995). Stochastic resonance and the benefits of noise - from ice ages to crayfish and squids. Nature *373*, 33–36.

Wilson, R.I., and Laurent, G. (2005). Role of GABAergic inhibition in shaping odor-evoked spatiotemporal patterns in the Drosophila antennal lobe. J. Neurosci. *25*, 9069–9079.

Wilson, R.I., Turner, G.C., and Laurent, G. (2004). Transformation of olfactory representations in the Drosophila antennal lobe. Science *303*, 366–370.